IOP Publishing Measurement Science and Technology
Meas. Sci. Technol. **31** (2020) 055008 (14pp) https://doi.org/10.1088/1361-6501/ab5131

Virtual topography measurement with transfer functions derived by fitted time series models

A Keksel[1,3], A P Lohfink[2], M Eifler[1], C Garth[2] and J Seewig[1]

[1] Institute for Measurement and Sensor-Technology, Technische Universität Kaiserslautern, Germany
[2] Scientific Visualization Lab, Technische Universität, Kaiserslautern, Germany

E-mail: keksel@mv.uni-kl.de

Received 17 July 2019, revised 14 October 2019
Accepted for publication 25 October 2019
Published 31 January 2020

Abstract

The deviations between the actual geometry of a workpiece and the measured geometry are defined by the transfer function of the surface topography measuring instrument used. When the transfer characteristics of a measuring instrument are known, they can, for example, be used for the estimation of measuring results by performing virtual measurements and can subsequently be applied for the estimation of the measurement uncertainty. A technique that has been increasingly applied for the determination of the transfer function of topography measuring devices is the approach based on physical modeling. Here, mathematical models apply simplifications of the complex physical relationships to describe the transfer characteristics of measuring devices. Another method used in practice is the application of material measures for the direct measurement of transfer properties. Within this paper, an alternative approach developed by the authors that applies the ARMA model is further investigated and optimized with regard to its practical applicability. This model was described in a previous publication (Keksel *et al* 2018 *Meas. Sci. Technol.* **29** 095012) and combines the advantages of theoretical modeling and the experimental determination of transfer characteristics. Within the present work, the approach is further optimized and it is demonstrated that the description of measuring devices by the ARMA model delivers reasonable results for various measuring principles that can be used for a precise virtual prediction of measurement results.

Keywords: ARMA filter, surface topography measuring device, transfer function, time series modeling, virtual measurement, geometrical product specification

(Some figures may appear in colour only in the online journal)

1. Introduction

Along with digitalization, the virtualization of industrial processes on different scales and levels has an increasing significance. This also applies to the field of Geometrical Product Specification (GPS). For the description of measuring devices, mathematical models that represent the complex physical relationships in a simplified manner are progressively being used [2]. This description does include the virtual measuring instrument, the virtual sample and the interaction between these two components, and can be applied to predict measurement results [2].

The prediction of measurement results can, for example, be used to analyze and optimize instrument setups and thus to increase the understanding of the underlying process, or even provide insights for the development of novel measuring systems [3, 4]. Furthermore, measurement data can be simulated by 'virtual measuring' and subsequently the measurement uncertainty can be established by a comparison with real measurement data [5]. Additionally, systematic errors

[3] Author to whom any correspondence should be addressed.

determined by virtual measurements can be corrected in the actual setup [2].

In literature, a multitude of approaches for the modeling of different virtual measuring devices are described. These include models for the description of stylus instruments [3], white light interferometers [6–8], scattering light sensors [8–11], atomic force microscopes [12] or x-ray computer tomographs [4, 13]. Knowing the underlying physical relationships, mathematical models can be used to simulate the transfer properties of different measuring devices and principles. In contrast to physical modeling, the practical machine-related characterization of measuring devices is based on material measures that can also be applied for uncertainty estimation [14]. Considering the determination of the transfer characteristics, examinations based on rectangular gratings [15], pseudo-random gratings [16], material measures that are designed in the frequency domain [17], spheres [18] or the super-fine roughness standards [19] have been carried out in order to provide test frequencies for the determination of the instrument behavior. However, typically the chirped standard [20–22] or the star-shaped groove material measure (Siemens Star) [14, 23, 24] are applied to determine the small scale fidelity limit or the lateral period limit respectively. Leach *et al* summarized different samples to perform according calibration procedures [25]. A detailed comparison of the Siemens star and the chirped standard was recently carried out [26].

A rather theoretical approach for the prediction of transfer behavior is the instrument transfer function (ITF) as described by de Groot *et al* [27]. Further theoretical considerations have been summarized by Foreman *et al* [28].

In previous work [1], the authors presented a method to determine the transfer properties of topography measuring devices on the basis of a model that combines findings from the measurement of a realistic engineering surface with a mathematical model (auto-regressive-moving-average or ARMA model). This combination enables a practical description of the transfer properties by an analytical model, which can be used to generate virtual measurement data. Within this paper, the applications of the ARMA-model are extended to other measuring principles and optimized with regard to their practical ability. In doing so, the application of the approach for virtual measuring with several measuring principles is described in depth.

2. The auto-regressive-moving-average model

We propose the application of the auto-regressive-moving-average model (ARMA model) for the determination of the transfer behavior of surface topography measuring devices. This method is used in several fields of application. In stochastic time series analysis, the ARMA model is commonly applied to predict the further course of a time series [29, 30]. In signal processing, digital ARMA filters, which are better known as infinite impulse response filters or IIR filters, are widely used [31, 32]. A further field of application of the ARMA model is the description of rough surfaces. Seewig proposed the utilization of this model for the frequency-dependent description of rough surfaces [33] and Eifler *et al* used the so-called ARMAsel approach [34–36] for the artificial generation of realistic technical surfaces [37]. In [1], the ARMA model was used to model the transfer characteristics of topography measuring devices. The transfer characteristics of topography measuring devices were modeled as a linear ARMA filter with the aid of real engineering surfaces, which were modeled as time series. The mathematical description of the according model is summarized in the following.

For a discrete time series $u[h]$ with $h = 1, 2, ..., N$ the ARMA model, with the coefficients $\mathrm{AR}[k]$ and $MA[l]$, and the degrees of freedom p, $q+1$ can be written as [29]

$$z[n] = -\sum_{k=1}^{p} \mathrm{AR[k]} \cdot z[n-k] + \sum_{l=0}^{q} \mathrm{MA}[l] \cdot u[n-l] \quad \text{with} \quad n = \begin{cases} p+1, \ldots, N & \text{if } p \geqslant q \\ q+1, \ldots, N & \text{else} \end{cases}. \tag{1}$$

This general approach for time series modeling is adapted to discretized surface profiles in a way that the actual surface profile (known as virtual data of the simulated manufacturing of a profile material measure) corresponds to u and the measured or respectively transferred dataset of a surface topography measuring instrument (measurement data) corresponds to z. The mathematical term $\sum_{k=1}^{p} AR[k] \cdot z[n-k]$ describes the auto-regressive part of the model while $\sum_{l=0}^{q} \mathrm{MA}[l] \cdot u[n-l]$ represents the moving-average part. Equation (1) can be transformed into the (spatial) frequency-domain by the discrete Fourier transform leading to the frequency-dependent description of the transfer from the actual surface to the measured surface:

$$Z(\Omega) = -Z(\Omega) \cdot \sum_{k=1}^{p} \mathrm{AR}[k] \cdot \mathrm{e}^{-\mathrm{i}\cdot\Omega\cdot k} + U(\Omega) \cdot \sum_{l=0}^{q} \mathrm{MA}[l] \cdot \mathrm{e}^{-\mathrm{i}\cdot\Omega\cdot l}. \tag{2}$$

Based on this consideration, the frequency-dependent transfer function $\upsilon(\Omega)$, with $\Omega = 2\pi \cdot \frac{m}{N}$ and $m = 0, 1, ..., N-1$, can be determined as [17]

$$\upsilon(\Omega) = \frac{Z(\Omega)}{U(\Omega)} = \frac{\sum_{l=0}^{q} \mathrm{MA}[l] \cdot \mathrm{e}^{-\mathrm{i}\cdot\Omega\cdot l}}{1 + \sum_{k=1}^{p} \mathrm{AR}[k] \cdot \mathrm{e}^{-\mathrm{i}\cdot\Omega\cdot k}}. \tag{3}$$

The $\mathrm{AR}[k]$ and $\mathrm{MA}[l]$ coefficients can be determined by an optimization approach. In [1], a least-squares optimization approach is suggested and derived in detail. Another commonly applied approach utilizes the Yule–Walker equations [30].

In previous investigations examined by the authors, it has been proven that the transfer behavior of topography measuring devices can be fully characterized by the $\mathrm{AR}[k]$ and $\mathrm{MA}[l]$ coefficients [1, 26]. However, as the proposed ARMA model is a linear model, it is to be expected that some nonlinear effects that influence the measured surface topography may not be fully representable by the model. Examples for such effects include the morphological filter effect of the stylus tip in tactile sampling [38] or effects based on diffraction when optical measuring instruments are considered [39]. Despite the precondition of linearity, it could be shown that the approach sufficiently delivers accurate results that

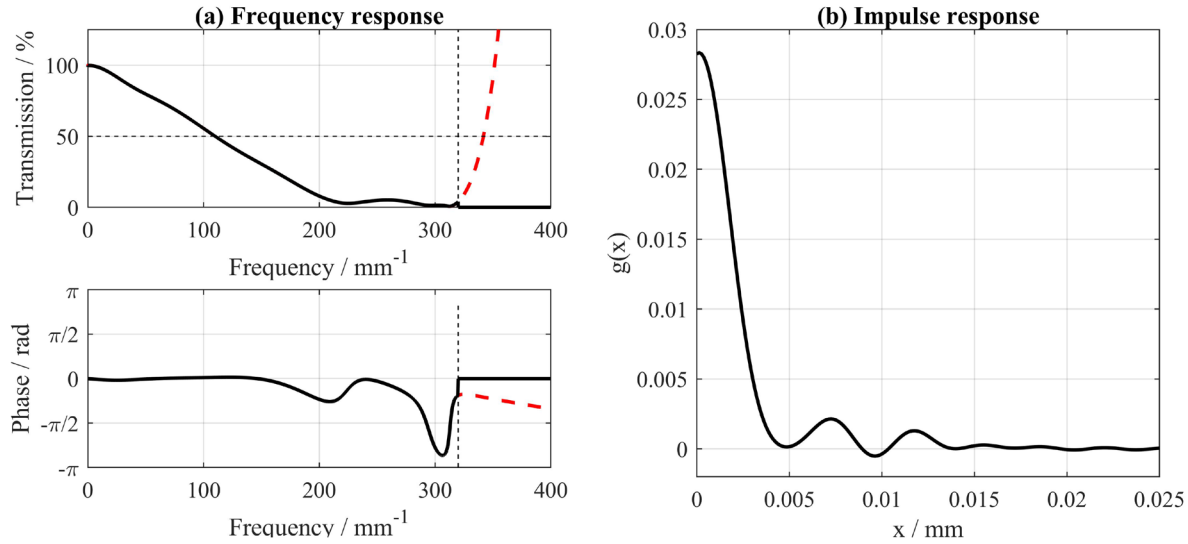

Figure 1. Filter properties of an ARMA-modeled filter represented by its (a) frequency response and (b) impulse response. The measuring device under consideration is a confocal microscope with a 20× lens (numerical aperture of NA = 0.45). The red dashed curve in (a) corresponds to the pure AR and MA coefficient-based frequency response, the black solid curve in (a) corresponds to the modified frequency response. The impulse response in (b) is generated on the basis of the modified frequency response.

describe the (linear) transfer behavior of investigated measuring devices (stylus instrument and confocal microscope) very well under certain conditions [1].

Figure 1 shows the filter properties of an ARMA filter modeled in [26] using the frequency response (amplitude and phase response) and the impulse response. The instrument modeled here is a confocal microscope with 20× magnification (NA = 0.45).

The frequency response in figure 1(a) corresponds to that of a low-pass filter with a cut-off frequency (spatial frequency at which the amplitude transmission equals 50%) of $f = 110\ \mathrm{mm}^{-1}$. The phase angle φ for low spatial frequencies ($f < 160\ \mathrm{mm}^{-1}$) is $\varphi \approx \pm 0$ rad. Only at higher spatial frequencies (partly only spatial frequencies in the range of measuring noise) larger deviations from $\varphi = 0$ rad can be observed. The modeled ARMA filter therefore describes an (almost) phase-true low-pass behavior (black solid line). The red dashed curve exceeding frequencies of $f = 320\ \mathrm{mm}^{-1}$ is the result of the frequency response representation on a pure basis of the determined AR and MA coefficients. Due to the digital resolution of the confocal microscope used, the frequency response is modified at frequencies $f \geqslant 320\ \mathrm{mm}^{-1}$ as due to the sampling theorem no amplitude transmission can be expected. The red dashed curve therefore indicates unphysical behavior of the frequency response of spatial frequencies $f \geqslant 320\ \mathrm{mm}^{-1}$ (Nyquist frequency) that are suppressed, leading to the black solid curve and an updated formulation of (3):

$$v(\Omega) = \sigma(\Omega_{\mathrm{Nyquist}} - \Omega) \cdot \frac{\sum_{l=0}^{q} \mathrm{MA}[l] \cdot \mathrm{e}^{-\mathrm{i}\cdot\Omega\cdot l}}{1 + \sum_{k=1}^{p} \mathrm{AR}[k] \cdot \mathrm{e}^{-\mathrm{i}\cdot\Omega\cdot k}} \text{ with } \sigma(t) = \begin{cases} 1 & t > 0 \\ 0 & \text{else} \end{cases}. \tag{4}$$

This procedure has been described in a previous publication [1] where the general feasibility of the approach was demonstrated. The approach will be adapted and enhanced in this paper. The impulse response of the ARMA filter under consideration (figure 1(b)) was generated using the modified transfer function (black solid line of figure 1(a)). The filter behavior modeled here was observed in similar ways when modeling other measuring instruments (optical and tactile) using the presented ARMA model. Further, the practical applicability of the ARMA model for the description of the transfer characteristics of topography measuring devices have been proven by comparing the fitted results with measured transfer characteristics [26]. The measured results were acquired with the Siemens star and the chirped standard [26], both material measures that are typically applied for this task (see section 1). The objective of the present publication is to make the approach applicable for virtual measurements and to evaluate the practical abilities of the ARMA model for this task. Thus, the approach is optimized with respect to the input and modeling parameters and applied to several other measuring principles.

3. Used measuring devices, measuring object and signal pre-processing

For the implementation of equation (1), measurement data as well as reference data of the measured surface topography are required. In other words, the actual topography, which serves as the input of the measuring device (reference data), must be known. Measuring objects that meet this requirement are material measures that are utilized to characterize the measurement uncertainty and to ensure the traceability route [14]. Within this paper, a material measure that was designed to calibrate the *Rk*-parameters as defined in ISO 13565-2 [40] is used [41]. The ARMA modeling approach for characterizing the transfer behavior requires a special pre-processing of the measurement data and the reference data [1]. An optimized data pre-processing is subsequently derived. Further, the influence of different modeling parameters on the results is

Table 1. An overview of the utilized measuring principles for the described study.

No.	Measuring principle	Resulting topography
1	Stylus instrument (SI) $r_{tip} = 5$ µm	Profile
2	Chromatic confocal sensor (CCS) NA = 0.7	Profile
3	Confocal microscope (CM) (a) 20× /NA = 0.45, (b) 50× / NA = 0.5, (c) 100× /NA = 0.95	Areal
4	White light interferometer (WLI) (a) 20× /NA = 0.4, (b) 50× / NA = 0.55, (c) 100× /NA = 0.85	Areal

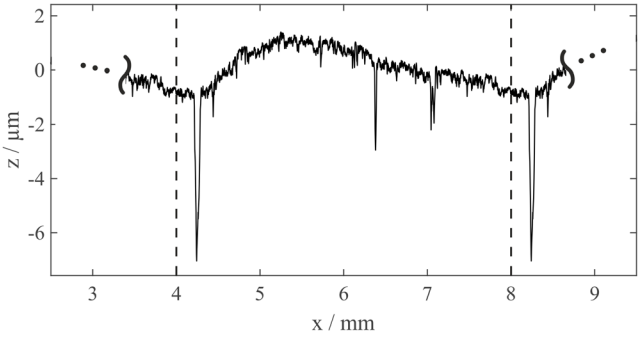

Figure 2. Characteristic profile of the *Rk*-calibrated rough surface.

investigated in order to enhance the abilities of the approach for virtual measurements.

3.1. Measuring devices

For a comprehensive description of the suitability of the proposed ARMA model for the determination of the transfer behavior, four different instruments/principles were used. Table 1 gives an overview regarding the utilized measuring principles and configurations.

3.2. Measuring object: Rk-calibrated rough surface

The *Rk* material measure developed at the Institute of Measurement and Sensor-Technology at the Technische Universität Kaiserslautern represents a stratified surface, which was designed on the basis of a cylinder running surface from industrial practice [41, 42]. The profile is shown in figure 2 and was designed with a model-based approach that considers influences from manufacturing and measuring. The processes are modeled for the design process and include virtual manufacturing and measuring based on morphological filtering that introduce a bandwidth limitation to the sample [41]. Just as many other profile material measures, the sample was manufactured with an ultra-precision turning process [17].

The *Rk*-calibrated sample contains 3.2 periodic continuations of the 4.0 mm profile as shown in figure 2, resulting in a total length of 12.8 mm. In [1] it was shown that this material

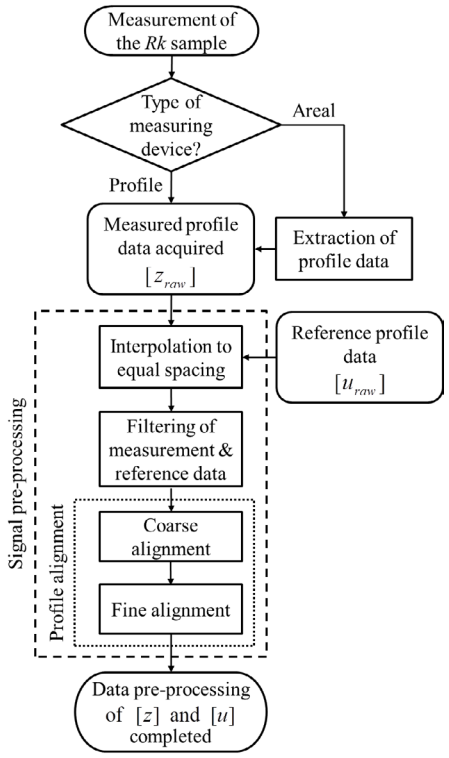

Figure 3. Signal pre-processing flowchart.

measure in particular is well-suited for the modeling of the transfer behavior of topography-measuring instruments due to its surface structure, although it was not designed for this purpose. This is due to the significant provision of both low and high spatial frequencies. Thus, the pre-processing of the modeling approach will be further optimized based on the chosen sample.

3.3. Signal pre-processing

In order to apply the fit of the ARMA model, a pre-processing of the measurement (input) and reference (output) data is required. Both profile and areal measurement data are obtained from the devices described in section 3.1. From the areal data, profiles are extracted and undergo the same pre-processing as the profile measurement data. The pre-processing of the measurement and reference data is divided into several steps, which are described below and visualized in figure 3.

3.3.1. Interpolation to equal spacing. In general, the raw measurement and reference data differ in sampling distance. To use the proposed ARMA model, measurement and reference profiles are linearly interpolated under consideration of the sampling theorem. The influence of the spacing size Δx (interpolated resolution) on the modeling result is part of the subsequent investigation.

3.3.2. Filtering. The filtering of the profile measurement data is performed considering the recommendations in ISO 25178-3 [43] and ISO 3274 respectively [44]. This specifies guide values for the nesting index λ_s for the filtering of tactile

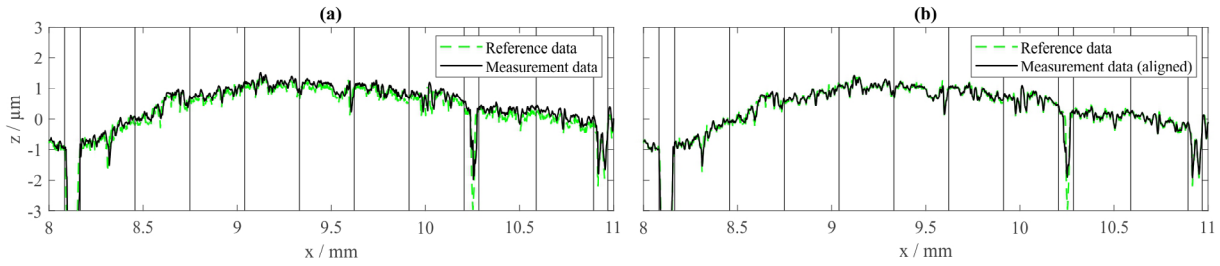

Figure 4. The first step of data pre-processing—coarse adjustment. (a) Offset-free measurement data versus reference data, (b) coarse adjusted measurement data versus reference data.

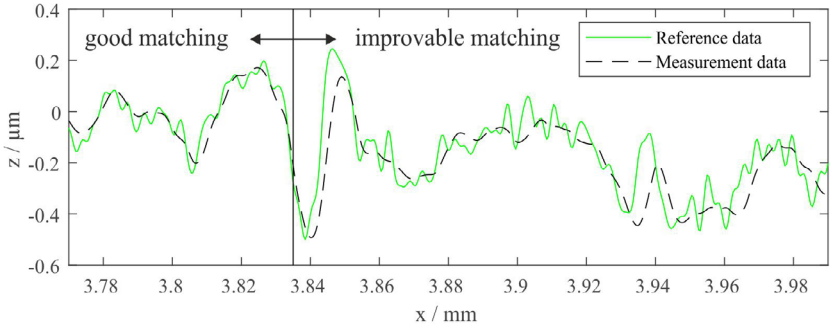

Figure 5. Example of a local mismatch.

or optically measured (areal) profiles in order to remove measurement noise from the signal. In addition to the filtering of the measured signal, the spatial frequencies that cannot be theoretically resolved by the individual measuring device are filtered out of the reference signal prior to modeling. This is done by setting the Fourier coefficients for frequencies $f \geqslant f_{\max}$ to zero (step-like transition function), where $f_{\max}$ is the largest frequency that can be sampled (Nyquist frequency) in the measured data set.

3.3.3. Alignment of the profiles. In order to process measurement and reference data in equation (1), their alignment to each other must be reasonable. Amongst others, due to linearity deviations of the device, the profiles (raw measurement data and reference data) do not match very well after measurement, even after the removal of height and inclination offsets. To optimize the alignment, the influences of linearity deviations of the instrument and other sources of error are minimized before ARMA modeling is conducted. The sophisticated alignment of the profiles to each other is divided into two steps: coarse and fine adjustment.

3.3.3.1.Coarse adjustment. In order to minimize the deviations in the superposition of the two datasets in the lateral and vertical direction, the measured profile is first divided into several segments. Within each of these segments, the correlation between measured and reference data is optimized. This is done by maximizing the cross-correlation through lateral displacement as well as maximizing the correlation coefficient by tilting, and the vertical displacement of the measured data segment to the same mean height as the corresponding reference data segment. An exemplary result of the first pre-processing procedure step is illustrated in figure 4.

The segmentation intervals must be chosen based on the deviations between the two data sets and the structure of the profile. Since the *Rk*-profile shows isolated deep grooves, which are not always imaged at full depth, especially with optical measurements, it is reasonable to detect them and to align them to the reference data set, decoupled from the rest of the surface. This is the first optimization step in pre-processing compared to [1]. A simplified form of the crossing-the-line segmentation algorithm of [45] is used for the detection of the grooves.

Despite the best possible alignment by coarse adjustment, locally limited mismatches remain (see figure 5). Areas in which the coarse adjustment delivers good results smoothly merge into areas of less good matchings. These local mismatches are corrected by the fine adjustment.

3.3.3.2.Fine adjustment. To further improve the matching of measurement and reference data, an approach for synchronizing similar curves locally is applied [46]. Pre-defined functionals are applied to the curves, providing a number of landmarks for each curve. These landmarks can, for example, be located at highly pronounced peaks or valleys. Based on these landmarks, a piecewise cubic matching function for the measurement data curve is determined, mapping associated landmarks to the reference location. To prevent the formation of discontinuities and keep curve characteristics, the used mapping function is required to be continuous and

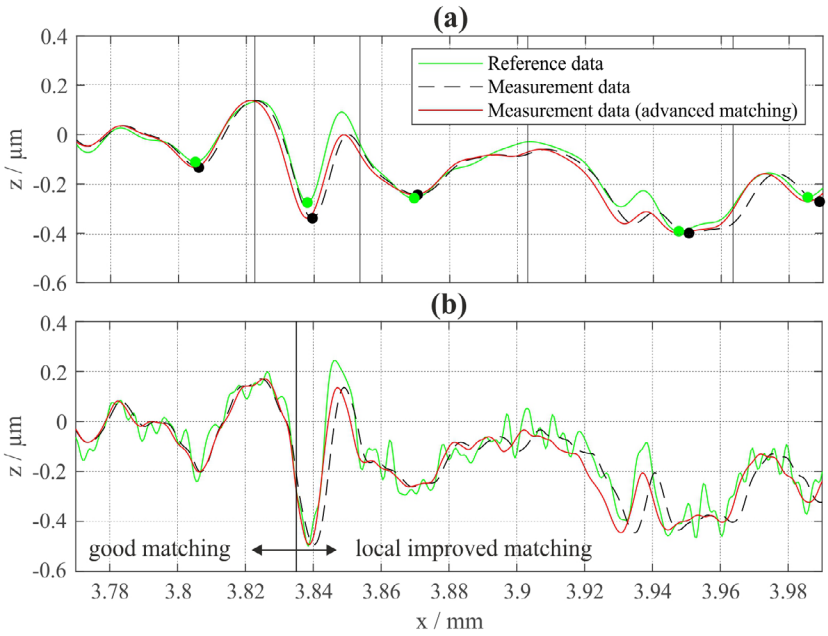

Figure 6. (a) Comparison of reference data, coarse adjusted measurement data and fine adjusted measurement data (all λ_s and λ_c filtered) with detected landmarks on measured and reference data (thick points). (b) Correction of local mismatch by fine adjustment.

monotonically increasing. This holds for the implemented monotone piecewise cubic interpolation as described by [47].

To avoid disturbances during landmark detection (pronounced peaks and/or valleys) by high frequencies or the average slope of the curve, a linear Gaussian low pass filter (nesting index λ_s) according to [48] and a double Gaussian filter (nesting index λ_c) according to ISO 13565-1 [49] are applied to the measurement and reference data before constructing the matching function to achieve a bandwidth limitation to the wavelengths that represent the roughness. The filtered measurement and reference data sets, as well as detected landmarks and the matched data set (matching function is applied to filtered measurement data) are exemplary illustrated in figure 6(a). Here, pronounced valleys serve as landmarks. Finally, the resulting matching function is applied to the unfiltered pre-adjusted measurement data to obtain the matched result. The final matching result can be found in figure 6(b).

The pre-processing described above is necessary for the success of ARMA modeling [1], which is examined below with respect to the modeling parameters and input profile length.

4. ARMA modeling—the influence of modeling parameters and input profile length

4.1. The influence of modeling parameters—degree of freedom and interpolated resolution

In order to optimize the ARMA model with regard to applications in virtual measuring, this section examines the extent to which the various modeling parameters affect the result quality. Assuming an optimized alignment of the measurement and reference data sets using the two-step matching algorithm presented in section 3.3, the influences of the following modeling parameters are examined: the number of AR and MA coefficients p and $q+1$, interpolated resolution Δx. These investigations are shown using stylus device measurements as an example, but the knowledge applies analogously to all measuring devices listed in table 1. The stylus measurement is chosen as a benchmark for the modeling results, since the transfer behavior of this principle, which corresponds to that of a low-pass filter, is described in detail in the literature, e.g. in [3, 38, 50], and is therefore well-known. Due to the finite radius of the probe tip, so-called morphological filtering occurs when scanning high spatial frequency structures, which is responsible for its low-pass characteristics. The cut-off frequency f_{limit} (spatial frequency at which 50% of the input amplitude is transferred) of the used stylus instrument is approximately $f_{\text{limit}} = 200\ \text{mm}^{-1}$ when measuring the structural amplitudes contained in the *Rk*-profile with a stylus tip radius of $r_{\text{tip}} = 5\ \mu\text{m}$ [1, 26]. A cut-off frequency close to $f_{\text{limit}} = 200\ \text{mm}^{-1}$ should therefore also be resulting using the ARMA model when the transfer behavior is adequately described by the model.

After pre-processing the measurement and reference data, ARMA modeling is performed by applying equation (1) in combination with the least-squares optimization method [1]. The result provides the AR coefficients $\text{AR}[k]$ with $k = 1, 2, \ldots, p$ and MA coefficients $\text{MA}[l]$ with $l = 0, 1, \ldots, q$, which represent the transfer behavior of the device used, when inserted in equation (4), taking into account the interpolated resolution. The number of AR and MA coefficients (p and $q+1$) define the degrees of freedom of the ARMA fit. The question, whether an underestimation or overestimation of the degrees of freedom affects the modeling result, immediately arises. The same applies to the interpolated resolution Δx. The lower resolution limit is specified by the sampling theorem, so no information contained in the raw measurement data is

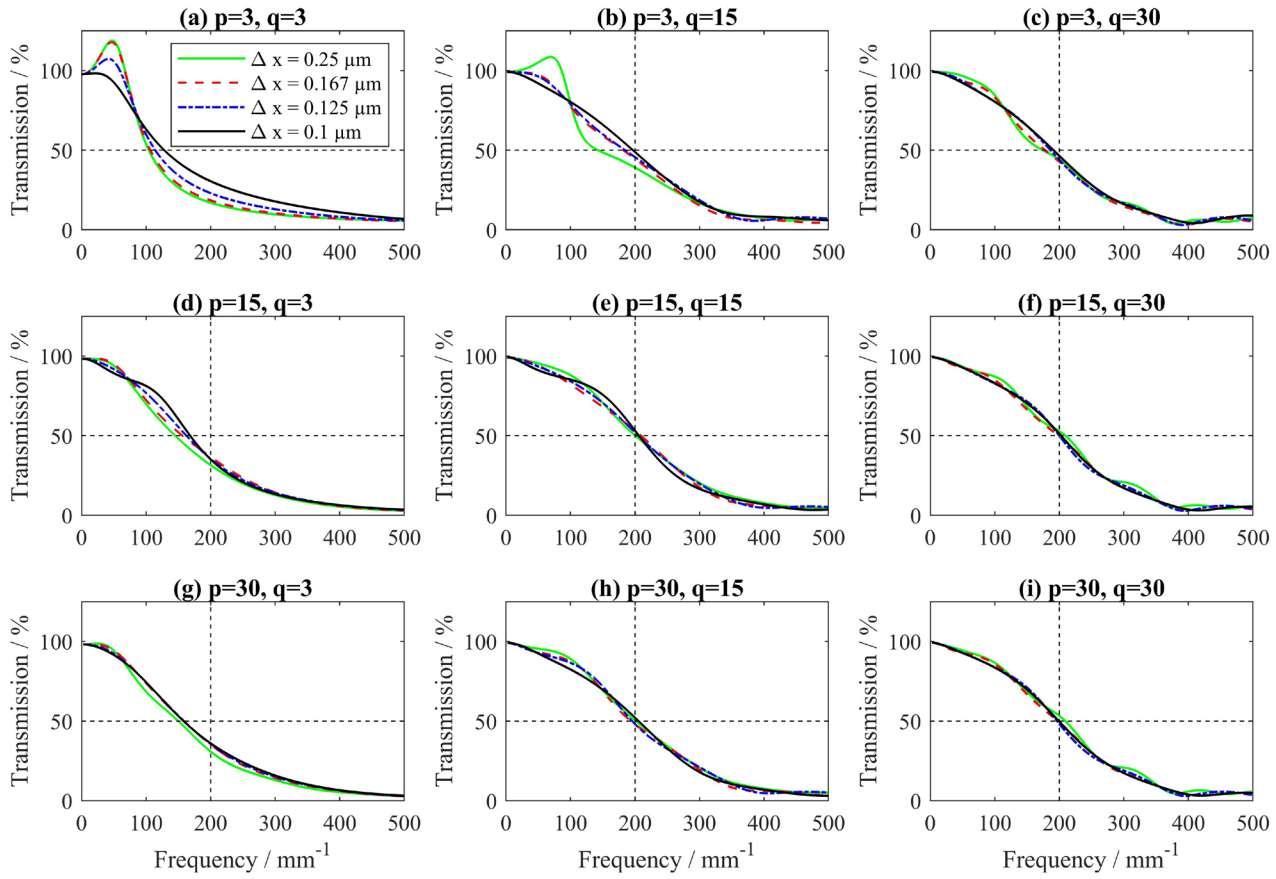

Figure 7. Transfer function estimation of a stylus device with a fitted ARMA model. Influence of degrees of freedom p and $q+1$, and resolution Δx on the resulting transfer function of the investigated device. (a) $p=3$, $q=3$, (b) $p=3$, $q=15$, (c) $p=3$, $q=30$, (d) $p=15$, $q=3$, (e) $p=15$, $q=15$, (f) $p=15$, $q=30$, (g) $p=30$, $q=3$, (h) $p=30$, $q=15$, (i) $p=30$, $q=30$.

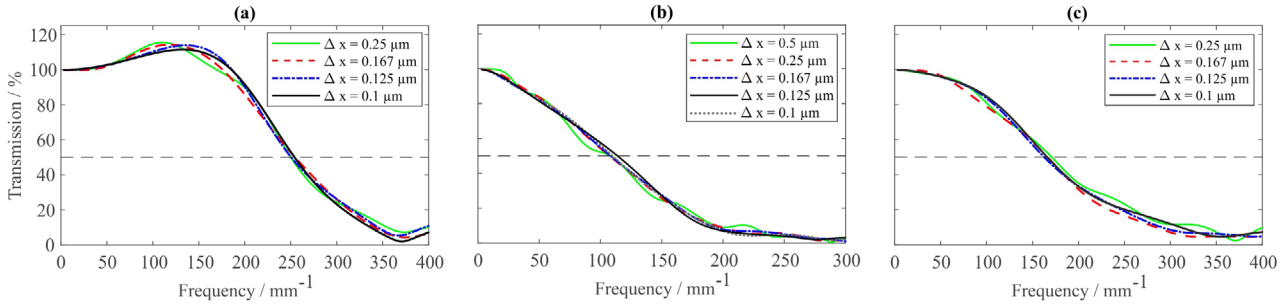

Figure 8. ARMA-modeled transfer function of (a) CCS, (b) CM 20× and (c) WLI 20× by using modeling parameters $p=30$, $q=30$ and different interpolated resolution Δx.

artificially rejected or falsified by undersampling. Figure 7 shows the result of transfer behavior modeling of the stylus device with respect to different degrees of freedom p and $q+1$, and different interpolated resolution values Δx.

The modeling result shown in figure 7 shows an increasing convergence from left to right and from top to bottom. When using a number of degrees of freedom that is too small, p or $q+1$ in (a), (b), (d) and (g), either a convergence behavior cannot be clearly observed and/or the determined spatial cut-off frequency $f_{\text{limit,ARMA}}$ deviates significantly from the expected value of $200\,\text{mm}^{-1}$. In (e), (f), (h), and most clearly in (i), a spatial cut-off frequency of approximately $f_{\text{limit,ARMA}} = 200\ \text{mm}^{-1}$ is visible at all resolutions Δx, which corresponds to the expected transfer behavior. When choosing p and q, be sure to choose enough coefficients. Concerning the resolution Δx, the recommendation is to oversample the signal by interpolation to equal spacing with *twice to five times* the Nyquist frequency. It should be considered that linear interpolation of a signal does not change its physical Nyquist frequency.

ARMA modeling of the other investigated measuring devices shows the same behavior. The modeled transfer functions of CM 20× (20× represent the lens magnification), WLI 20× and CCS with $p=q=30$ and different resolutions (taking into account the sampling theorem) are shown in figure 8.

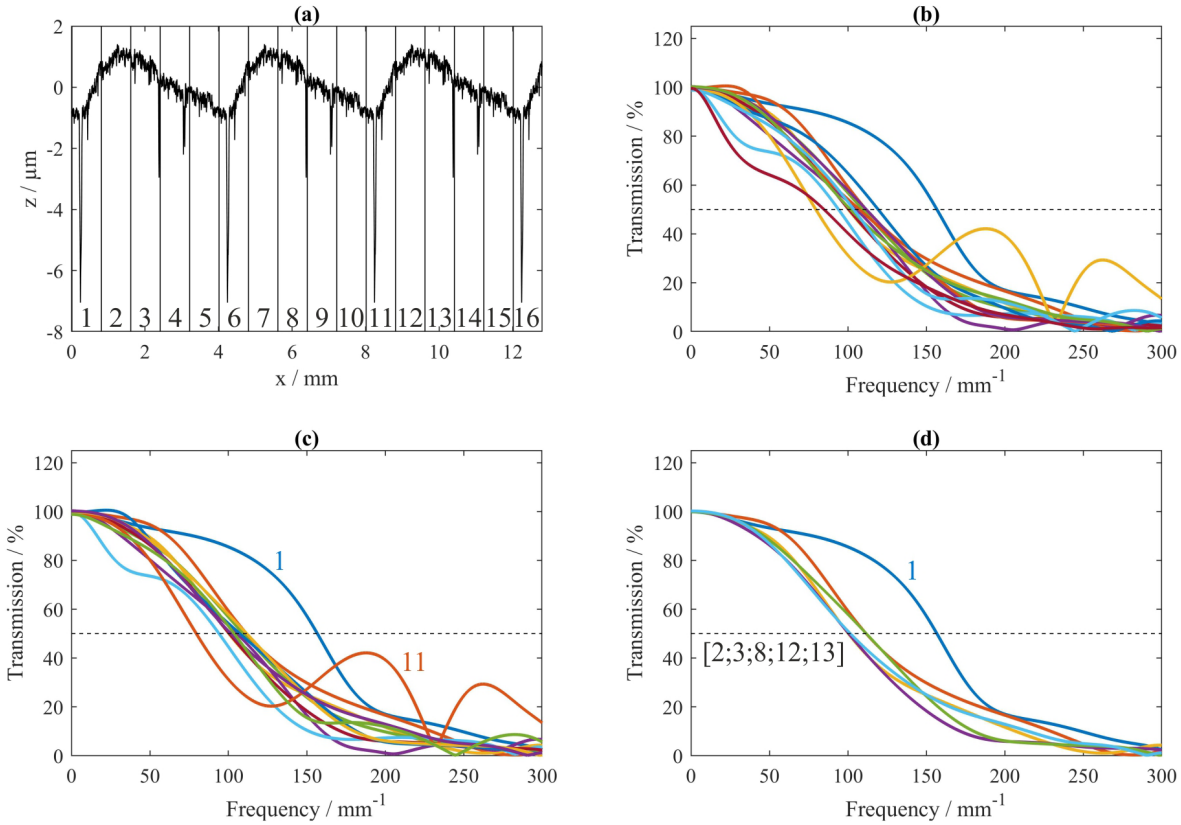

Figure 9. Results of CM 20× ARMA modeling by using a single image. (a) *Rk*-profile divided into 16 segments with a length of the field of view (800 µm). Single image-based modeling transfer functions based on profile segments, which fulfill different quality criteria—correlation coefficient (b) $r_{\mathrm{meas,ref}} > 0.5$, (c) $r_{\mathrm{meas,ref}} > 0.7$ and (d) $r_{\mathrm{meas,ref}} > 0.9$ for every subdivided interval.

4.2. Influence of the profile length

In the previous section, the total length of the manufactured *Rk*-profile was considered in the modeling. While a profile measurement of approximately 12.8 mm is easy to sample with stylus devices or optical point sensors, the areal acquisition is challenging. Using the confocal microscope with a 20× lens, for example, the field of view is equal to 800 × 800 µm². For the measurement of the total length of the *Rk* profile, at least 18 measurements are required, including one additional image at the beginning and at the end of the manufactured profile. When using a 50× lens (field of view size of 320 × 320 µm²) > 42, and when using a 100× lens (field of view size of 160 × 160 µm²) > 82 measurements are required. The measurement of such a large number of images is very time-consuming and at the same time causes uncertainties and artefacts due to the necessary stitching of the individual images, which should be avoided for practical purposes. How many images lead to a stable performance of ARMA modeling using the *Rk*-profile is investigated. In the ideal case, stable modeling is possible on the basis of the measured data of a single image.

First, the confocal microscope with a 20× lens is used to investigate whether a single image provides reasonable modeling results. For this purpose, the *Rk*-profile is divided into 16 segments, each corresponding to the field of view length of 0.8 mm (see figure 9(a)). On the basis of each of these segments, ARMA modeling is performed. For the alignment procedure, each of these segments is further subdivided into eight intervals. Based on these subdivided segments, the measurement profiles are aligned with the reference profiles.

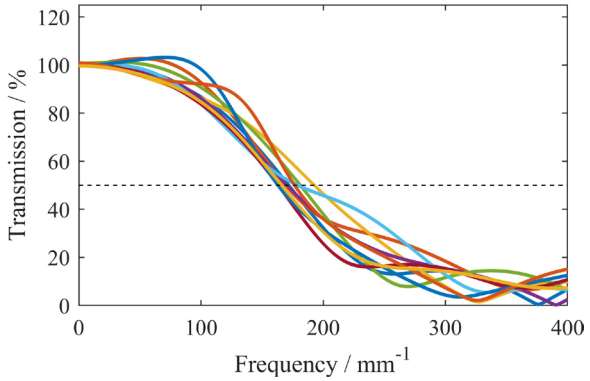

Figure 10. Results of WLI 20× ARMA modeling by using single images (quality criterion $r_{\mathrm{meas,ref}} > 0.9$ fulfilled by ten different profile segments).

Since the database for modeling on the basis of a single image is significantly smaller than when using the full profile length, the requirements on the local quality of the measurement, the quality of the profile alignment and the proper choice of the measuring location are considerably higher.

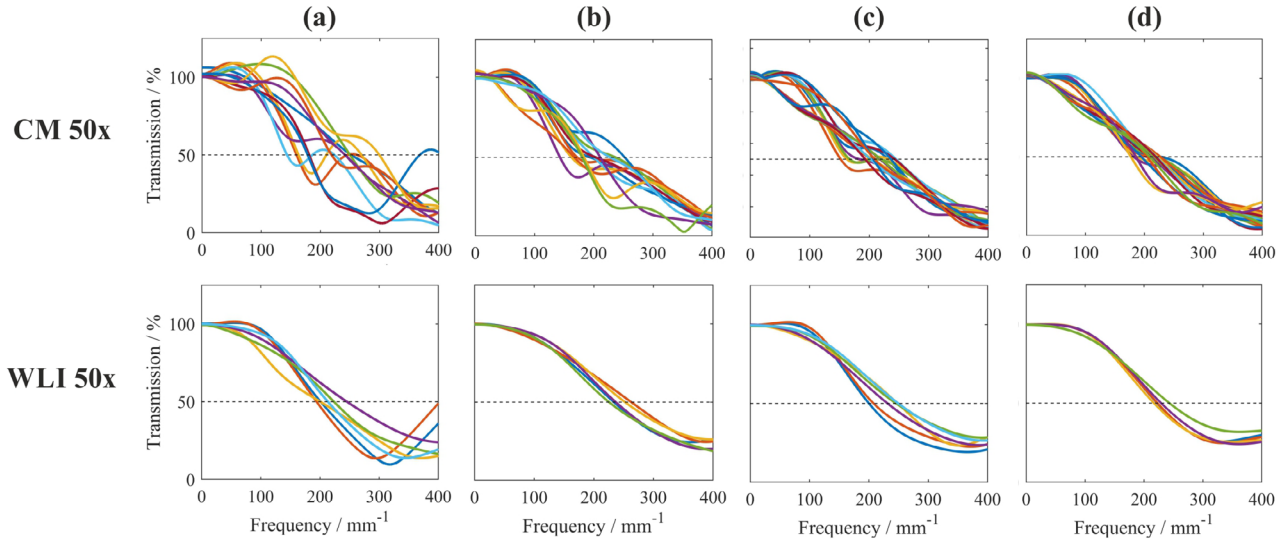

Figure 11. Results of CM 50× and WLI 50× ARMA modeling by using (a) a single, (b) two, (c) three and (d) four connected images.

While inaccuracies in alignment or short measurement lengths that are not representative for the transfer behavior can be compensated by using longer profiles, this is only possible to a limited extent when modeling is performed on the basis of very short profile segments.

For an estimation of the matching quality, the empirical correlation coefficient $r_{\mathrm{meas,ref}}$ of aligned measurement and reference profiles is calculated for each of the eight intervals within the investigated profile segment (length 800 µm, corresponds to the length of the field of view) after performing the two-step matching procedure. While larger deviations of the reference and measurement profile are still accepted as 'sufficiently good' ($r_{\mathrm{meas,ref}} > 0.5$, fulfilled by 14 profile segments) in figure 9(b), larger deviations are no longer accepted ($r_{\mathrm{meas,ref}} > 0.7$, fulfilled by 12 profile segments) in figure 9(c), and only 'very good' matching results ($r_{\mathrm{meas,ref}} > 0.9$, fulfilled by six profile segments) are accepted in figure 9(d). Accordingly, the transfer functions of (b)–(d) do not differ, but less well matching profiles that do not pass the quality test are not considered for ARMA modeling.

While in figure 9(b) the modeling results of the transfer function are still widely scattered, the transfer functions in figure 9(d) follow a very narrow corridor. The exception is the transfer function, which is based on the first segment. The profile matching provides very good results but this segment contains a relatively wide and deep groove, the measurement of which is not representative. The best matching results are provided by the segments on the 'dome' of the *Rk*-profile (segments 2, 3, 8, 12, 13). Modeling of transfer behavior on the basis of these segments corresponds to the behavior from figure 8(b) considering the total length of the *Rk*-profile. In the case of the confocal microscope in combination with a 20× lens it is therefore possible to model representative transfer behavior on the basis of a single image. For this purpose, however, it must be ensured that a suitable and representative measurement location has been chosen and that the quality of the measurement and matching is sufficiently good.

This is also valid for the measurement with a white light interferometer using a 20× Mirau lens (figure 10). Here, the field of view extends over 580 × 580 µm².

This quality pre-testing procedure is also applied to measurements with lenses of higher magnification (50× and 100×), so only profile matches with $r_{\mathrm{meas,ref}} > 0.9$ serve as a basis for ARMA modeling. By further reducing the length of the input profile, the available information for ARMA modeling decreases. Since the spatial frequency spectrum measurable by the measuring device used may no longer be fully represented in the measured field, it can be assumed that the modeled transfer behavior based on the measurement of a single image varies greatly at different measurement locations. For this reason, when 50× and 100× lenses are used, it is evaluated how the results differ when modeling is performed on the basis of (a) one, (b) two, (c) three and (d) four connected images. The results for the CM and WLI with a 50× lens (field of view 320 × 320 µm² and 232 × 232 µm²) are shown in figure 11 and the results using a 100× lens (field of view 160 × 160 µm² and 116 × 116 µm²) are shown in figure 12.

For all measuring device/lens combinations used here, it is determined that the different transfer functions modeled are characterized by a higher degree of congruency to each other with increasing input profile length. Furthermore, the modeling results represent plausible transfer characteristics in comparison with measurements performed by the authors [26]. For robust and reproducible modeling results, the 50× and 100× devices examined here require input profile lengths of at least two (WLI 50×), three (CM 100×) or four (CM 50×, WLI 100×) images with limited field of view respectively. When modeling on the basis of a single image, the results highly depend on local influencing factors. A good averaging of the transfer behavior cannot be guaranteed on the basis of such short input profiles. The extent to which the modeling results achieved here reflect realistic conditions is investigated in the next section using virtual measurements.

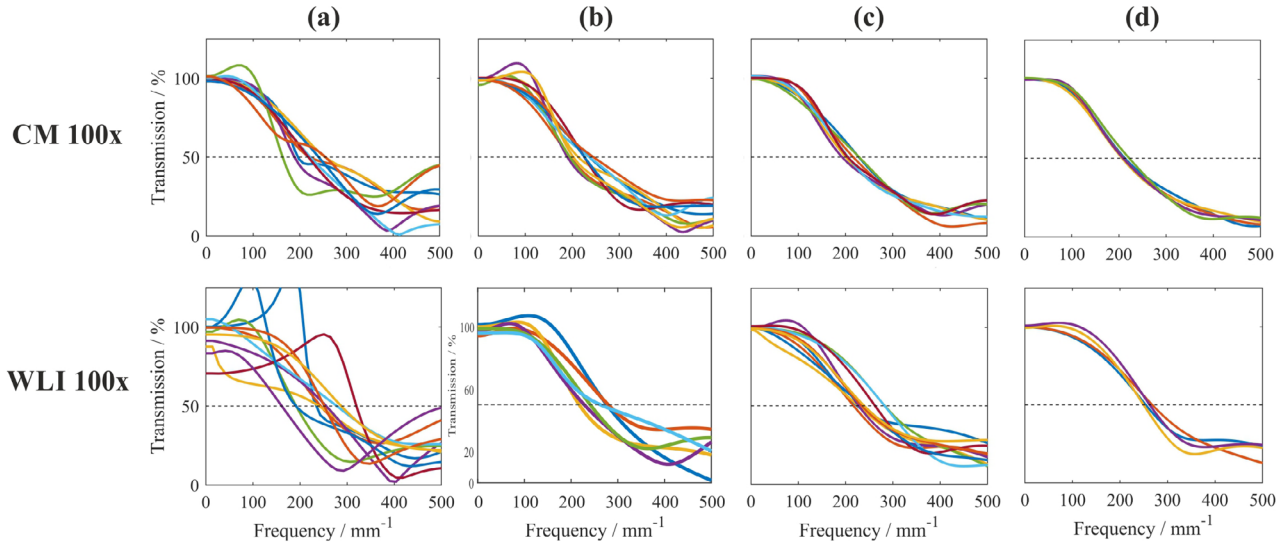

Figure 12. Results of CM 100× and WLI 100× ARMA modeling by using (a) a single, (b) two, (c) three and (d) four connected images.

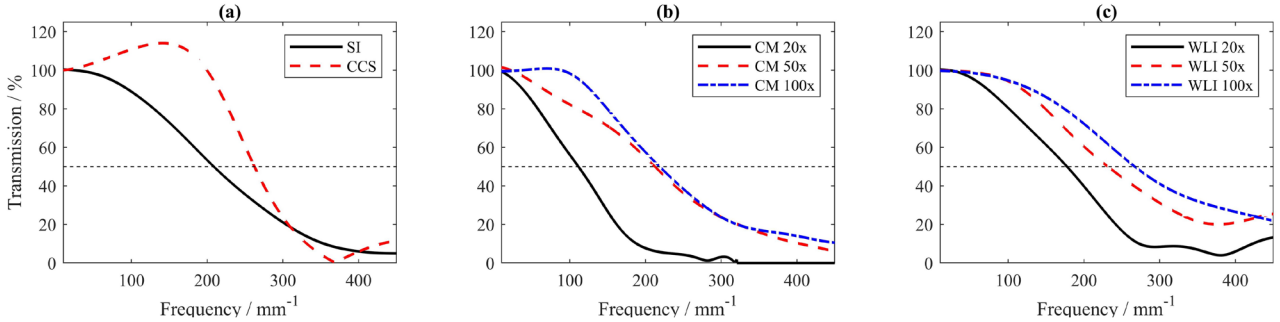

Figure 13. Reproducibly determined transfer functions of (a) stylus instrument SI and chromatic confocal sensor CCS, (b) confocal microscope CM and (c) white light interferometer WLI.

5. Virtual measurements

It was shown that the transfer characteristics of profile and areal topography measuring devices can be reproducibly determined with the aid of the ARMA model by measuring a few (connected) or even one image. The extent to which the achieved transfer functions represent reality is investigated in this section. For this purpose, representative transfer functions are determined for each of the examined measuring devices and virtual measuring is performed. By comparing the virtual and real measurement data, statements about the plausibility of the determined transfer behavior can be made. Figure 13 shows examples of reproducibly determined transfer functions. For the profile measurements (SI and CCS), an input profile length of 4 mm was used for ARMA modeling. For areal measurements (CM and WLI), the input profile length corresponds to the length of four connected images. In the previous section it was shown that this input profile length is sufficient even at high magnifications.

The evaluation of the similarity of virtual and real measurement is based on a defined quality criterion and on the visual comparison of both profiles. The quality criterion $L_{1,\,\mathrm{gradient}}$ is defined as

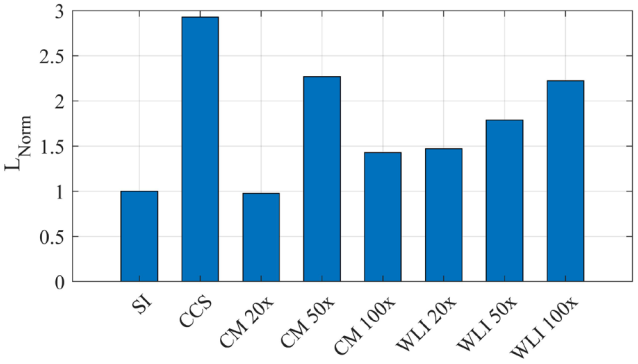

Figure 14. Comparison of real and virtual measurements based on quality criteria L_{Norm} ($L_{1,\mathrm{gradient}}$ normalized by $L_{\mathrm{SI,\,1,gradient}}$) for the different measuring devices examined.

$$L_{1,\,\mathrm{gradient}} = \frac{\sum_{i=1}^{n-1} \left| \frac{\Delta z_{\mathrm{virtual}}[i]}{\Delta x} - \frac{\Delta z_{\mathrm{measurement}}[i]}{\Delta x} \right|}{n} \quad \text{with} \quad \Delta z[i] = z[i+1] - z[i]. \tag{5}$$

The quality criterion $L_{1,\,\mathrm{gradient}}$ corresponds to the average absolute difference of the profile gradients of both profiles and provides a quantitative measure to compare the quality of

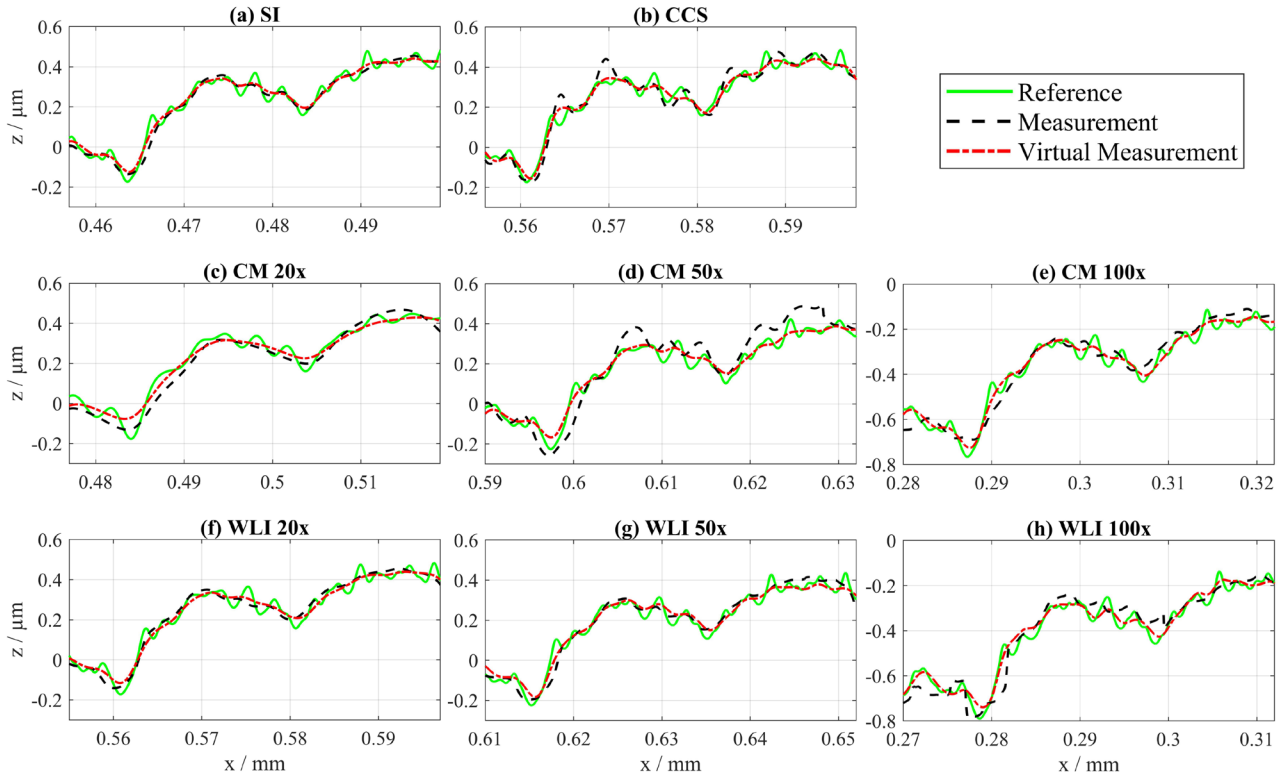

Figure 15. Direct comparison of reference, real measurement and virtual measurement based on derived transfer functions (figure 13) for examined measuring devices (table 1). (a) SI, (b) CCS, (c) CM 20×, (d) CM 50×, (e) CM 100×, (f) WLI 20×, (g) WLI 50×, (h) WLI 100×.

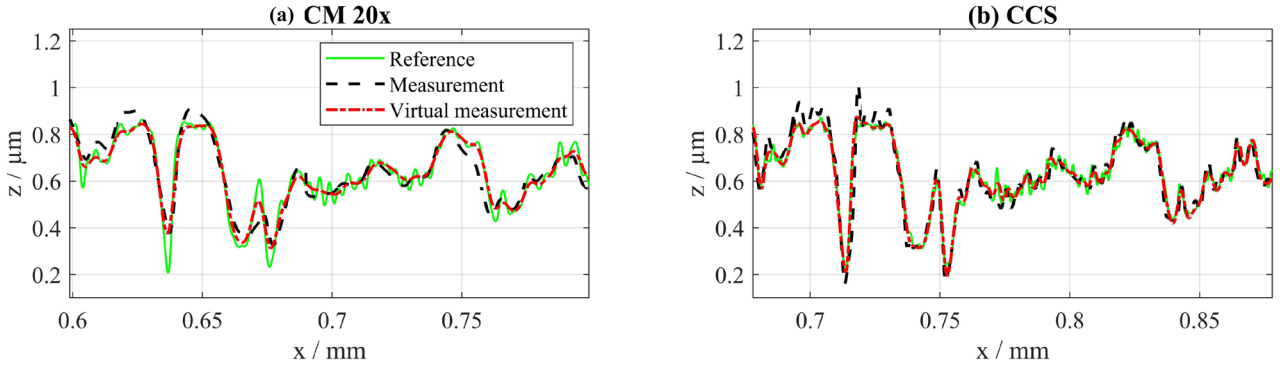

Figure 16. Comparison of real and virtual measurements of (a) CM 20× and (b) CCS.

the results for different measuring devices, see figure 14. The imaged quality criterion L_{Norm} is normalized by $L_{\mathrm{SI,\,1,gradient}}$ as the stylus instrument provides the highest level of agreement between the virtual and actual measurement. Since the tactile stylus method is well-known and well-controlled, it serves as a benchmark for the other models.

According to figure 14, the model for CM 20× ($L_{\mathrm{CM20\times,\,Norm}} \approx 1$) fits the reality best and the model for CCS fits it least well ($L_{\mathrm{CCS,\,Norm}} \approx 3$). The other investigated devices are located in the intermediate range with quality values of $1.4 < L_{\mathrm{Norm}} < 2.4$. To confirm the significance of L_{Norm}, exemplified sections of real and virtual measurements of the *Rk* material measure are directly compared in figure 15.

Figure 15(c) confirms the realistic results for CM 20×. The gradients of virtual and real measurement show a high level of congruence with each other and so the structures of the reference profile are transferred in a similar way. The models of WLI 20×, WLI 50× and CM 100× (figures 15(e)–(g)) show realistic transfer behaviors as well. Merely the models of CCS, CM 50× and WLI 100× (figures 15(b), (d) and (h)) show significant deviations from reality due to several local defects (WLI 100×, CM 50×) or overshoots (CCS). The causes for the observed pronounced overshoots in confocal microscopy were described based on the local surface curvature by Mauch *et al* [51]. In the model of the CCS (figure 13(a)), the overestimation of amplitude transmission was generally detected, but the overestimation of the profile amplitude in the real measurement is locally much more pronounced than in the virtual measurement. When comparing virtual and real measurements of WLI

Table 2. Comparison of *Rk* values of real and virtual measurements of CM 20× and CCS. The nominal values of the material measure are $Rk = 0.4$ µm, $Rpk = 0.15$ µm and $Rvk = 1.2$ µm.

	CM 20×			CCS		
	Measurement	Virtual measurement	Difference (%)	Measurement	Virtual measurement	Difference (%)
Rk (µm)	0.385	0.381	0.99	0.424	0.402	5.21
Rpk (µm)	0.144	0.134	6.74	0.164	0.140	14.50
Rvk (µm)	1.234	1.223	0.86	1.184	1.205	1.82

100× (figure 15(h)), a reasonable transfer function is determined on the one hand, which is plausible with regard to the characteristic transfer functions of the WLI 20× and WLI 50× (figure 13(c)) but, on the other hand, the direct comparison suggests deviations between real and virtual measurement. This presumed contradiction is due to the fact that the measurement of the WLI 100× shows local defects that distort the characteristic value $L_{\mathrm{WLI\,100\times,Norm}}$ strongly, but can be well compensated by ARMA modeling. At other locations, where the local measurement quality is high, the gradients of real and virtual measurement are similar, which confirms the general plausibility of the determined transfer behavior. The same applies to a limited extend for the CM 50× model.

Nevertheless, all models of the investigated measuring devices derived by the ARMA model, from the best (CM 20×) to the model with the largest deviations (CCS), show a high agreement with the real measurements. This can be observed in figure 15 and in more detail in figure 16 by comparing the results of CM 20× and CCS.

Furthermore, in order to provide another integral measure for the quality of the virtual measurements, the functional parameters represented by the *Rk* values according to [40] that are calibrated with the utilized material measure are determined and compared for the real and virtual measurements in table 2.

In this comparison, it can be observed that the resulting roughness parameters are in good agreement. The differences are in the nanometer-range and feature values between 4 and 24 nm. To further classify the quality of these results, they are compared with a set of measurements from a comparison with the *Rk*-calibrated surface (see [17]): when the same sample was measured with nine different stylus instruments, standard deviations of 3–11 nm for *Rk*, 2–7 nm for *Rpk* and 12–125 nm for *Rvk* were measured just as well as a systematic scattering of the mean values between 0.357–0.395 µm for *Rk*, 0.152–0.170 µm for *Rpk* and 1.133–1.264 µm for *Rvk*. The magnitudes of both the systematic and the stochastic measurement uncertainty illustrate the quality of the virtual measurement: the deviations between the virtual measurements and real measurements are in the scale of a typical stochastic measurement uncertainty of a stylus measuring device. The systematic deviations between different devices that use the same measuring principle are significantly larger even compared to the virtual measurements of the device with the largest deviations.

6. Conclusion

For the transfer function determination in surface topography measurement, numerous approaches have been researched. In previous examinations, the authors have suggested the utilization of time series models (ARMA-model) [1]. In the present work, the approach was enhanced for additional measuring principles and optimized with regard to is practical applicability for virtual measuring. First, the measuring devices/principles to be modeled and the *Rk*-calibrated profile that served as a sample were presented. The pre-processing procedure of the measurement data was optimized by integrating a structural analysis of the measured profile into the algorithm to enhance the alignment of the model input data.

Based on the optimized pre-processing algorithm, it was examined which criteria the modeling parameters have to meet in order to achieve meaningful transfer functions. The modeling parameters were identified as number of AR and MA coefficients and the interpolated resolution of the input data. It turned out that both the number of degrees of freedom (number of AR and MA coefficients) and the interpolated resolution has a lower threshold value that should be exceeded.

In the next step, the ARMA modeling procedure was examined for virtual measuring. Since the measurement of large profiles with optical areal surface topography measuring devices is challenging, the minimum length of the input profile was determined so that the modeling of the transfer behavior is reproducible and stable. It was shown that stable modeling based on a single image (field length between 580 and 800 µm) is possible with objectives of small magnifications (20×). For higher magnifications (50×, 100×), approximately four individual images with lengths of the field of view between 116 and 320 µm are required for performing reproducible modeling.

Based on these results, representative transfer functions of the examined measuring instruments were determined and used for virtual measurements. When comparing virtual and real measurement data, the determined transfer behavior of the individual measuring devices generally reflects reality well and single outliers or defects in the measurement data can be compensated. The deviations between virtual and real measurements are within the range of a typical stochastic measuring uncertainty.

The ARMA model, which combines the advantages of real measurements and theoretical modeling, has proven to be a useful addition to the existing purely experimental or

theoretical methods for determining the transfer characteristics of topography measuring devices. In future examinations, the presented virtual measuring approach will be extended by the indication of an uncertainty range based on the physical modeling of measuring processes.

Acknowledgment

This research is funded by the Deutsche Forschungsgemeinschaft (DFG, German Research Foundation)—252408385—IRTG 2057.

ORCID iDs

A Keksel https://orcid.org/0000-0001-7779-4687
M Eifler https://orcid.org/0000-0001-6628-7284

References

[1] Keksel A, Eifler M and Seewig J 2018 Modeling of topography measuring instrument transfer functions by time series models *Meas. Sci. Technol.* **29** 095012
[2] Schmitt R *et al* 2008 Virtuelle Messgeräte: definition und Stand der Entwicklung (virtual measuring instruments: definition and development status) *Tech. Mess.* **75** 298–310
[3] Puente León F and Beyerer J 2005 Oberflächencharakterisierung durch morphologische Filterung *Tech. Mess.* **72** 663–70
[4] Hilpert U, Bartscher M, Bellon C, Jaenisch G-R, Staude A and Goebbels J 2008 Einfluss von Signal-Rausch-Verhältnis und Binning auf die Formmesseigenschaft eines CT-Messsystems—Vergleich von Messergebnis und Simulationen, Poster 11, St. Gallen, DACH-Jahrestagung (https://www.ndt.net/article/dgzfp2008/Inhalt/p11.pdf)
[5] Schwenke H and Trapet E 1999 Abschätzung von Messunsicherheiten durch Simulation an Beispielen aus der Fertigungsmesstechnik *Dissertation* Physikalisch-Technische Bundesanstalt, Braunschweig
[6] Schmitt R *et al* 2008 Modellierung optischer Messprozesse: Untersuchung der Interferenzmikroskopie mittels Simulation (Modelling of optical measurement methods: analysis of interference microscopy via simulations) *Tech. Mess.* **75** 230–6
[7] de Groot P and Colonna de Lega X 2004 Signal modeling for lowccoherence heightcscanning interference microscopy *Appl. Opt.* **43** 4821–30
[8] Torner F M 2018 Entwicklung virtueller, optischer Sensoren zur Charakterisierung geometrischer Oberflächen *Dissertation* Technische Universität Kaiserslautern, Kaiserslautern
[9] Seewig J, Eifler M, Schneider F, Kirsch B and Aurich J C 2016 A model-based approach for the calibration and traceability of the angle resolved scattering light sensor *Surf. Topogr.* **4** 024010
[10] Torner F, Stelzer G, Anslinger L and Seewig J 2017 Description and evaluation of a simplified model to simulate the optical behavior of an angle-resolved scattered light sensor *J. Comput. Inf. Sci. Eng.* **17** 021003
[11] Torner F, Das J, Stelzer G, Linke B and Seewig J 2017 Fundamental analysis of the usability of an angle-resolved scattered light sensor for monitoring vibratory finishing processes based on ray tracing simulations *Appl. Mech. Mater.* **869** 115–27
[12] Xu M, Dziomba T and Koenders L 2011 Modelling and simulating scanning force microscopes for estimating measurement uncertainty: a virtual scanning force microscope *Meas. Sci. Technol.* **22** 094004
[13] Bellon C and Jaenisch G-R 2007 aRTist—analytical RT inspection simulation tool *Proc. DIR 2007—Int. Symp. on Digital Industrial Radiology and Computed Tomography (Lyon, France, 25–27 June 2007)*
[14] ISO 25178-70 2014 *Geometrical Product Specifications (GPS)—Surface Texture: Areal—Part 70: Material Measures* (International Organization for Standardization)
[15] Krüger-Sehm R, Frühauf J and Dziomba T 2005 Determination of the short wavelength cutoff of interferential and confocal microscopes *Proc. Metrol. Prop.* **10** 21–8
[16] Yashchuck V V, McKinney W R and Takacs P Z 2008 Binary pseudorandom grating standard for calibration of surface profilometers *Opt. Eng.* **47** 073602
[17] Eifler M 2016 Modellbasierte Entwicklung von Kalibriernormalen zur geometrischen Produktspezifikation *Dissertation* Technische Universität Kaiserslautern, Kaiserslautern
[18] Su R, Wang Y, Coupland J M and Leach R K 2017 On tilt and curvature dependent errors and the calibration of coherence scanning interferometry *Opt. Express* **25** 3297–310
[19] Ehret G, Schulz M, Brand U, Koenders L, Krüger-Sehm R, Dziomba T, Dai G, Felgner A and Meeß R 2011 Optische und taktile Oberflächencharakterisierung auf der nm-Skala *PTB Mitt.* **121** 142–51
[20] Krüger-Sehm R, Bakucz P, Jung L and Wilhelms H 2007 Chirp-Kalibriernormale für Oberflächenmessgeräte (chirp calibration standards for surface measuring instruments) *Tech. Mess.* **74** 572–6
[21] Pehnelt S, Osten W and Seewig J 2011 Comparative analysis of optical surface measuring systems with a chirp calibration standard *Tech. Messen* **78** 457–62
[22] Seewig J, Eifler M and Wiora G 2014 Unambiguous evaluation of a chirp measurement standard *Surf. Topogr.* **2** 045003
[23] Giusca C L and Leach R K 2013 Calibration of the scales of areal surface topography measuring instruments: part 3. Resolution *Meas. Sci. Technol.* **24** 105010
[24] Tan Ö 2012 Characterization of micro- and nanometer resolved technical surfaces with function-oriented parameters *PhD Thesis* Friedrich-Alexander Universität, Erlangen-Nürnberg
[25] Leach R K, Giusca C, Haitjema H, Evans C and Jiang X 2015 Calibration and verification of areal surface texture measuring instruments *CIRP Ann.* **64** 797–813
[26] Eifler M, Keksel A and Seewig J 2019 Comparison of material measures for the determination of transfer characteristics of surface topography measuring instruments *Surf. Topogr.* **7** 015024
[27] de Groot P and Colonna de Lega X 2005 Interpreting interferometric height measurements using the instrument transfer function *Proc. of FRINGE* (Berlin: Springer) pp 30–7
[28] Foreman M R, Giusca C L, Török P and Leach R K 2013 Phase-retrieved pupil function and coherent transfer function in confocal microscopy *J. Microsc.* **251** 99–107
[29] Patterson K 2011 *Unit Root Tests in Time Series* vol 1 (Basingstoke: Palgrave Macmillan) (https://doi.org/10.1057/9780230299306)
[30] Vogel J 2015 *Prognose von Zeitreihen—Eine Einführung für Wirtschaftswissenschaftler* (Wiesbaden: Springer) (https://doi.org/10.1007/978-3-658-06837-0)
[31] Meyer M 2014 *Signalverarbeitung: Analoge und digitale Signale, Systeme und Filter* vol 7 (Wiesbaden: Springer) (https://doi.org/10.1007/978-3-8348-8138-0)
[32] Schmidt H and Schwabl-Schmidt M 2014 *Digitale Filter: Theorie und Praxis mit AVR-Mikrocontrollern* (Wiesbaden: Springer) (https://doi.org/10.1007/978-3-658-03523-5)

[33] Seewig J 2000 *Praxisgerechte Signalverarbeitung zur Trennung der Gestaltabweichungen technischer Oberflächen* (Aachen: Shaker)
[34] Broersen P M T 2000 Facts and fiction in spectral analysis *IEEE Trans. Instrum. Meas.* **49** 766–72
[35] Broersen P M T and Wensink H E 1993 On finite sample theory for autoregressive model order selection *IEEE Trans. Signal Process.* **41** 194–204
[36] Broersen P M T 1998 The quality of models for ARMA processes *IEEE Trans. Signal Process.* **46** 1749–52
[37] Eifler M, Ströer F, Rief S and Seewig J 2018 Model selection and quality estimation of time series models for artificial technical surface generation *Technologies* **6** 3
[38] Krystek M 2004 Morphological filters in surface texture analysis *Proc. of the XI Int. Colloquium on Surfaces ICS (Chemnitz)* pp 43–55
[39] Xie W, Hagemeier S, Bischoff J, Mastylo R, Manske E and Lehmann P 2017 Transfer characteristics of optical profilers with respect to rectangular edge and step height measurement *Proc. SPIE* **10329** 1032916
[40] ISO 13565-2 1996 *Geometrical Product Specifications (GPS)—Surface Texture: Profile Method; Surfaces Having Stratified Functional Properties—Part 2: Height Characterization Using the Linear Material Ratio Curve* (International Organisation of Standardization)
[41] Seewig J, Eifler M, Schneider F and Aurich J C 2016 Design and verification of geometric roughness standards by reverse engineering *Proc. CIRP* **45** 259–62
[42] Seewig J, Eifler M, Hüser D and Meeß R 2019 Rk material measure—a model based design *Tech. Mess.* **86** 478–86
[43] ISO 25178-3 2012 *Geometrical Product Specifications (GPS)—Surface Texture: Areal—Part 3: Specification Operators* (International Organization for Standardization)
[44] ISO 3274 1997 *Geometrical Product Specifications (GPS)—Surface texture: Profile Method—Nominal Characteristics of Contact (Stylus) Instruments* (International Organization for Standardization)
[45] Seewig J, Scott P J, Eifler M and Hüser D 2019 Crossing-the-line segmentation as a basis for roughness parameter evaluation *Int. Conf. on Metrology and Properties of Engineering Surfaces* 22
[46] Kneip A and Gasser T 1992 Statistical tools to analyze data representing a sample of curves *Ann. Stat.* **20** 1266–305
[47] Fritsch F N and Carlson R E 1980 Monotone piecewise cubic interpolation *SIAM J. Numer. Anal.* **17** 238–46
[48] ISO 16610-21 2011 *Geometrical Product Specifications (GPS)—Filtration—Part 21: Linear Profile Filters: Gaussian Filters* (International Organization of Standardization)
[49] ISO 13565-1 1998 *Geometrical Product Specifications (GPS)—Surface Texture: Profile Method—Surfaces Having Stratified Functional Properties—Part 1: Filtering And General Measurement Conditions* (International Organization for Standardization)
[50] Bodschwinna H and Hillmann W 1992 *Oberflächenmeßtechnik mit Tastschnittgeräten in der industriellen Praxis. 1. Aufl* (Berlin, Köln: Beuth)
[51] Mauch F, Lyda W and Osten W 2013 Model-based assistance system for confocal measurements of rough surfaces *Proc. SPIE* **8788** 87880U